OPEN ACCESS
OPUS AUGSBURG

Universität Augsburg
Universitätsbibliothek

# Self-healing graphene-based composites with sensing capabilities

**Eleonora D'Elia, Suelen Barg, Na Ni, Victoria G. Rocha, Eduardo Saiz**

**Angaben zur Veröffentlichung / Publication details:**

D'Elia, Eleonora, Suelen Barg, Na Ni, Victoria G. Rocha, and Eduardo Saiz. 2015. "Self-healing graphene-based composites with sensing capabilities." *Advanced Materials* 27 (32): 4788–94. https://doi.org/10.1002/adma.201501653.

**Nutzungsbedingungen / Terms of use:**

**licgercopyright**

*Dieses Dokument wird unter folgenden Bedingungen zur Verfügung gestellt: / This document is made available under these conditions:*
***Deutsches Urheberrecht***
*Weitere Informationen finden Sie unter: / For more information see:*
*https://www.uni-augsburg.de/de/organisation/bibliothek/publizieren-zitieren-archivieren/publiz/*

# Self-Healing Graphene-Based Composites with Sensing Capabilities

*Eleonora D'Elia, Suelen Barg, Na Ni, Victoria G. Rocha, and Eduardo Saiz**

Natural systems are a rich source of scientific inspiration. Skin for example functions as an efficient protective barrier for the human body that is able to sense the external environment and repair autonomously. The translation of these physiological properties to synthetic materials could open new opportunities in many strategic fields from health care to robotics. Significant progress has been achieved in the development of materials able to sense and/or self-repair.[1,2] The latter often relies on the use of an external stimulus to trigger healing[3] or on the use of vascular[1,4] or capsule-based[5] systems for the storage and release of healants upon damage. However, these systems often show incomplete healing, cannot heal multiple times, or require the prompt location of the damage site. An alternative is the use of supramolecular polymers (macromolecular aggregates cross-linked by dynamic covalent or hydrogen bonds) that provide an efficient path toward autonomous, repeatable self-healing.[6] Still, the integration of healing and functional capabilities in strong and lightweight materials remains a challenge. In this work, we confine a supramolecular polymer in a graphene ultralight network to form robust, electrically conductive composites able to self-repair. These composites can sense pressure and flexion and fully restore their properties after damage multiple times and without an external stimulus.

Polyborosiloxane (PBS) is a supramolecular polymer that exhibits an intrinsic self-healing character due to its dynamic dative bonds (created via triple and quadruple bonds between Boron and the Oxygen in the Si—O groups). However, PBS is a well-known "solid–liquid" material whose viscoelastic properties (it flows as a highly viscous liquid at low strain rates but behaves as a solid at high strain rates) promote fast and complete healing but impair structural applications (**Figure 1**a,b).[7] In order to impart electrical conductivity and increase strength, we have used standard homogenization techniques to disperse reduced graphene oxide (rGO) flakes in PBS. The composite remains electrically insulating even with rGO contents as high as 10 wt%. This result is in agreement with previous calculations[8] of the percolation threshold for high aspect ratio platelets, and the problem increases by flake crumpling and agglomeration. In addition, the material still exhibits a shear-thickening "solid–liquid" behavior with storage (G′) and loss modulus (G″) comparable to PBS (**Figure 2**a). Other authors have also observed that PBS retains its "solid–liquid" behavior even after relatively large additions of graphene oxide or clay nanoplatelets.[9]

To overcome these limitations, we have confined the self-healing polymer in rGO networks with microscopic porosity. The networks are prepared through the freeze casting of graphene oxide (GO) suspensions followed by thermal reduction.[10,11] The technique uses the directional freezing of the suspensions to form networks with a characteristic structure formed by long channels (hundreds of microns) packed in a honeycomb arrangement. The channels, templated by the ice crystals, are aligned along the direction of ice growth. Their diameter is of the order of ≈10–20 μm and they are separated by thin (below 50 nm) carbon walls formed by an accumulation of entangled rGO flakes bonded together by physical forces (Figure 1). The final densities of the networks range between 2 and 11 mg $cm^{-3}$, depending on the concentration of the starting GO suspensions. Their compressive yield strengths increase with density between 1 and 30 kPa. Due to their hydrophobic nature, the rGO scaffolds can be fully infiltrated with a solution of poly(dimethylsiloxane) (PDMS) and boron oxide nanoparticles to form "in situ" the PBS polymer. The final rGO content of the composites is very low, and varies between 0.2 and 1 wt%.

The rGO network acts as a skeleton that confines PBS and impedes its flow. The storage modulus of the composite is up to two orders of magnitude higher than PBS alone or with dispersed rGO flakes. More importantly, it has a solid behavior (G′ > G″) in the whole range of frequencies analyzed (Figure 2b). The graphene network also acts as a continuous electrical path providing electrical conductivities up to 90 S $m^{-1}$ (Figure 1c).

The tensile behavior of the composites is highly dependent on the strain rates and they can reach strengths up to 0.2 MPa at the faster rates (50 mm $min^{-1}$, Figure 2). The strain-dependence results from the shear-thickening behavior of the confined PBS (Figure 2). This is strongly dictated by the B—O dynamic covalent bonds that form the viscoelastic polymer network (**Figure 3**).[12,13] While at low strain rates the polymer flows as a viscous fluid (due to a more loose arrangement of the polymer segments) at fast strain rates the network gets tighter and the polymer becomes elastic, breaking in a more brittle manner.[13,14] When the test is carried out at lower rates (typically below 10 mm $min^{-1}$) the composite exhibits large elongations to fracture due to the viscous behavior of the polymer.

The mechanical response depends on the molecular weight of the polymer (Figure 2d). The use of a low molecular weight (LMw) polymer (circa 1000 Da) results in a stiffer and more brittle material. Conversely, even if showing lower maximum

E. D'Elia, Dr. N. Ni, Dr. V. G. Rocha, Prof. E. Saiz
Centre for Advanced Structural Ceramics
Department of Materials
Imperial College of London
London SW7 2AZ, UK
E-mail: e.saiz@imperial.ac.uk
Dr. S. Barg
The School of Materials
The University of Manchester
Oxford Road, Manchester M13 9PL, UK

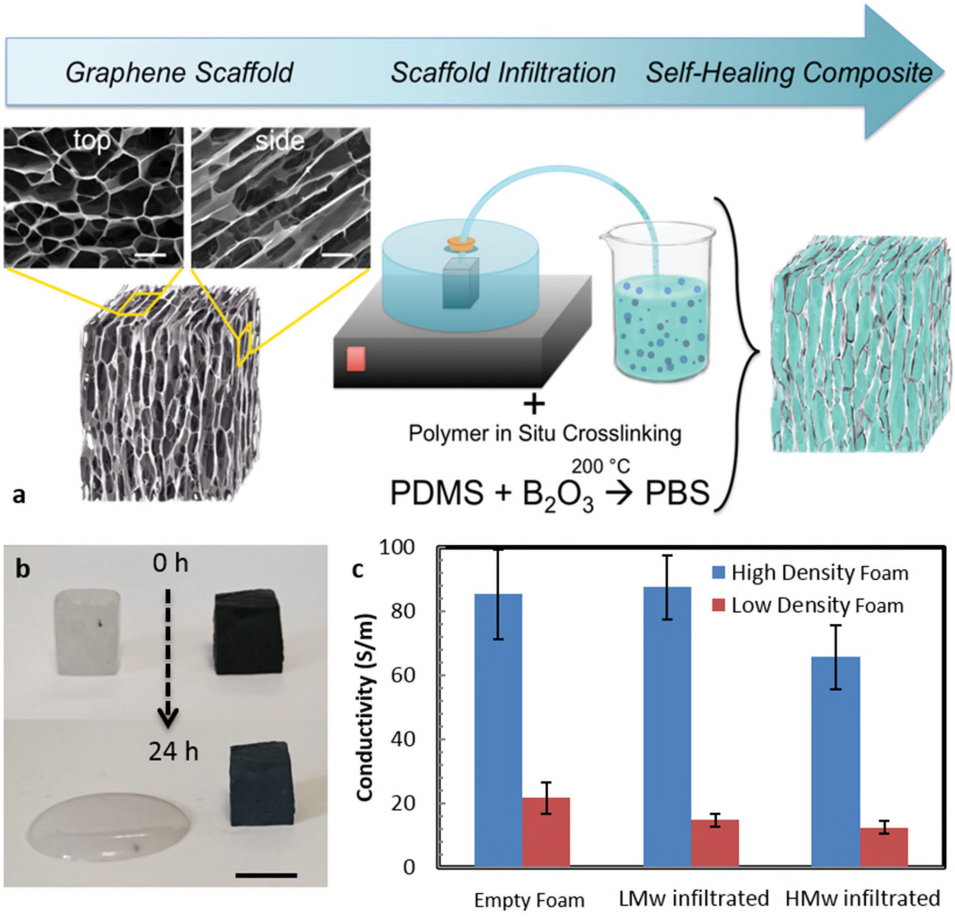


**Figure 1.** Processing, mechanical stability, and electrical conductivity. a) From left to right: ultralight reduced graphene oxide (rGO) networks contain microscopic channels separated by thin walls and packed to form a honeycomb cross-section (scale bar: 20 μm). The scaffolds are infiltrated with a PDMS/$B_2O_3$ solution via vacuum casting. Cross-linking of the polymer into PBS takes place in situ by heating the infiltrated networks at 200 °C. The resulting composites are composed of an rGO continuous network confining PBS. Infiltration is complete and the residual porosity in the composite is less than 1%. b) Mechanical stability. Optical images showing the flow behavior of polymer-only (left) and composite samples (right) of equal size and shape. After only a few hours in air at room temperature the "solid–liquid" polymer flows due to its viscoelastic properties forming a film that spreads on the substrate whereas the composite formed by the polymer confined in the graphene network retains its structure (scale bar: 1 cm). c) Effect of network density (low density, 2.5 ± 0.2 mg $cm^{-3}$, high density 11 ± 1 mg $cm^{-3}$) and PBS molecular weight (low: 25 cSt (LMw) and high: 65 cSt (HMw)) on the electrical conductivity of the composites. The conductivity can reach values up to 90 S $m^{-1}$ for materials fabricated from high-density networks as their graphene content is larger. Expansion of the network after polymer infiltration may reduce conductivity slightly.

strength, a higher molecular weight polymer (circa 3500 Da) leads to values of work of fracture 10 times higher (Figure 2). This is due to the intrinsic stiffness that a shorter-chain polymer imparts to the material, as no de-entanglement of chains occurs during extension. When using the high molecular weight (HMw) polymer, the work of fracture is higher and the composite can reach strains 10 times larger (around 100%).

Upon fracture or damage, the "solid–liquid" polymer is released (Figure 3). Healing results from the combination of dynamic bond re-formation in PBS with polymer flow and the resulting capillary forces that re-establish physical contact between the fractured network walls. As a result the composite is able to recover its mechanical and electrical properties (**Figure 4**). Damage at different levels from surface to deep scratches (few hundred microns in depth and width, Figure 4) or complete ruptures can be efficiently repaired. Cut samples can heal autonomously and fully recover their mechanical and electrical properties by just placing their surfaces in contact without additional pressure (Figure 4). In contrast to other materials,[15] no external stimulus, i.e., temperature or pressure, is required for self-healing. Samples broken in tension recover autonomously above 80% of their strength by placing the fracture surfaces in contact at ambient conditions for 10 min (Figure 4). Complete recovery is achieved in only 1 d. Electrical conductivity is also recovered after cutting the sample in half and subsequently putting the parts back together without additional pressure. The composites fabricated using the LMw polymer recover above 90% of their original conductivity in only few minutes (Figure 4).

The polymer wets rGO and the resulting capillary forces are able to physically reconnect the network walls exposed during fracture (Figure 3) to restore electrical conductivity (Figure 4). Once healing is achieved, the polymer is re-encapsulated in the graphene scaffold to form a robust, solid composite. Since

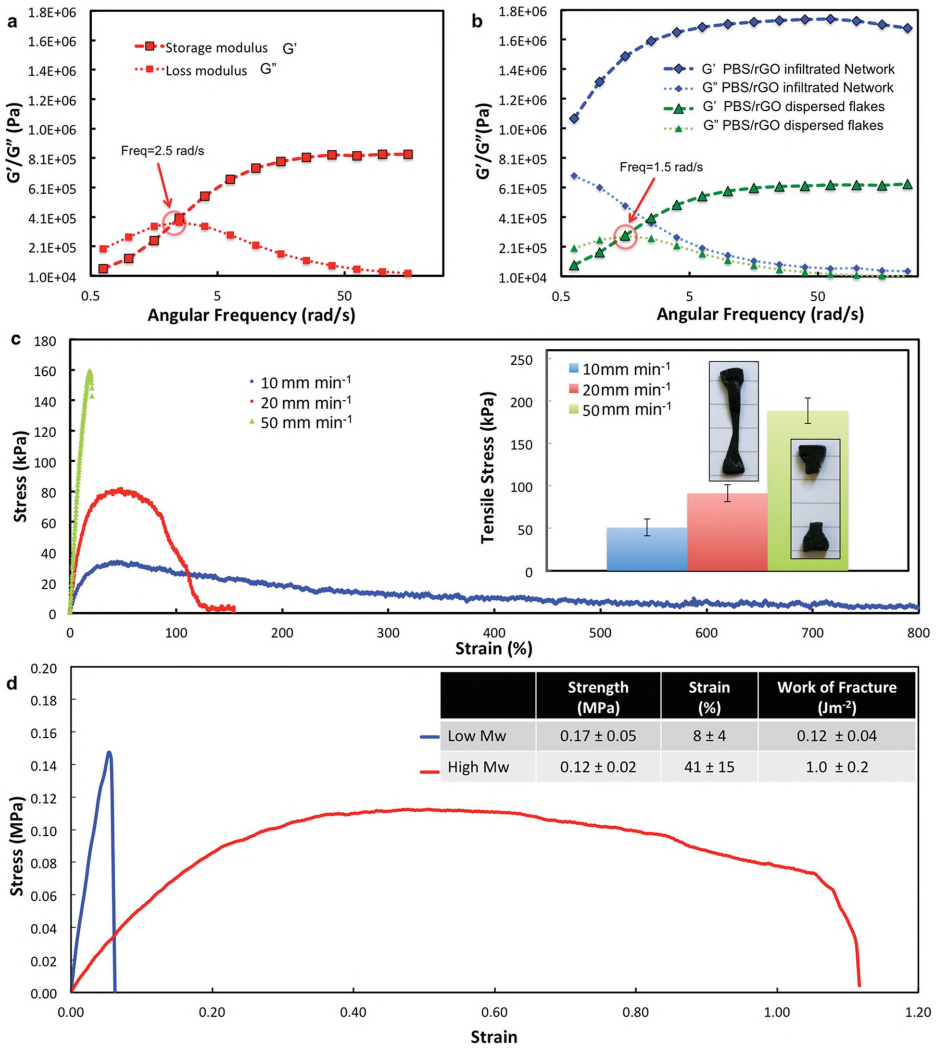


**Figure 2.** Mechanical performance. a) Viscoelastic properties of PBS. The polymer exhibits a shear-thickening behavior, with the storage modulus (G′) surpassing the Loss modulus (G″) at high frequencies (crossover point at 2.5 rad $s^{-1}$). b) Viscoelastic properties of the rGO scaffolds/LMw-polymer composite and LMw-polymer with dispersed graphene flakes (rGO content 0.5 wt% in both cases). While the composite produced by infiltrating a graphene network exhibits a solid-like behavior for the entire frequency range, the composite produced by the dispersion of graphene in the polymer shows a shear-thickening behavior similar to the polymer itself a), with a crossover point at 1.5 rad $s^{-1}$. c) Typical tensile stress/strain curves of the composites at different strain rates showing stronger responses and less elongation for higher rates. c,inset) Tensile strength as a function of strain rate. Dog-bone shape fractured samples (inset) show the change in the fracture behavior. d) Typical stress/strain curves for composites made out with polymers of two different molecular weights (1000 vs 3500 Da, LMw and HMw, respectively).

healing is driven by polymer flow and by the dynamic dative bond driven interactions between polymer chains (Figure 3), the healing agent does not get exhausted. Self-repair can be repeated multiple times; we have performed 6–8 healing cycles in the experiments reported in this work with no loss of structural healing capabilities (Figure S4, Supporting Information). Unlike many other materials, structural healing is not reduced after exposing the fracture surfaces to the environment for prolonged periods of time. Surfaces left exposed to the open air for over 1 d could heal as much as freshly cut material (Figure S5, Supporting Information). The density of the starting graphene foam does not have a noticeable effect on the healing kinetics and mechanical healing does not seem to be affected by the molecular weight of the polymer in the time scale of the experiments. Composites fabricated with both polymers recover their strength after 1 d. However, molecular weight has a noticeable effect in electrical healing. While composites fabricated with LMw polymer regain almost all their conductivity the recovery is much lower in the case of materials prepared using HMw PBS (Figure 4d). The difference may be due to a lower density of cross-links in the supramolecular network of the HMw PBS that results in faster flow. While this flow promotes mechanical healing, it can result in partial coating of the exposed graphene walls, therefore hampering electrical connection.

During tensile-electrical tests the composite remains conductive even at strains up to 30%. Loss of conductivity coincides

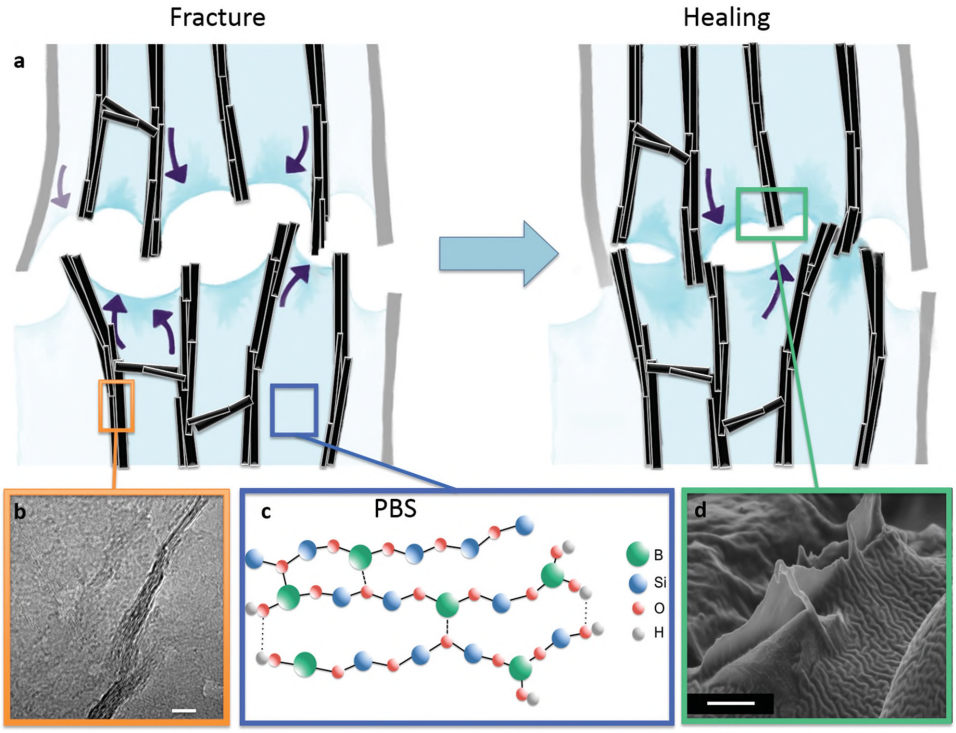


**Figure 3.** a) Schematic of the healing process. b) The network walls are formed by entangled graphene flakes (transmission electron micrograph). c) The healing nature of the PBS network is given by the spontaneous formation of dynamic bonds between the boron and the oxygen on a silicone backbone (of a dative nature) and the formation of hydrogen bonds due to the residual OH-groups at the end of some of the unreacted polymer chains. This reversible cross-linking is relatively fast and does not require any external stimulus. d) Fracture exposes the carbon walls of the network (scanning electron micrograph of a fracture surface). Capillary forces resulting from polymer flow bring the wall together re-establishing the connection between the network walls while the reversible bonds in the polymer enable full healing in the matrix. Scale bars: b) 1 nm, d) 2 μm.

with the fracture of the composite (**Figure 5**a). These experiments suggest that the graphene scaffold in the composite can strain much more after having been infiltrated with PBS. One explanation for this behavior could be that the polymer enables the rearrangement and sliding of the graphene walls in the composite during tension while retaining their connection.

The mechanical and electrical properties of the self-healing composites allow the preparation of bulk materials and films able to sense deformation and mechanical forces, i.e., pressure and flexion (Figure 5). Sensing is based on the measurable variation of voltage/resistance with strain. Tactile pressure sensitivity can be monitored using a cyclic compression test while measuring the voltage variations in a four-point probe configuration. Under a compression of ≈200 kPa, the measured voltage becomes noticeably higher. Buckling and deformation of the graphene network increase the length of the conductive path. Upon release, the voltage gradually decreases in 10–20 s to the initial value. The small increase in voltage at zero pressure after the first cycles relates to the residual nonelastic deformation of the composites, as well as to the kinetics of recovery (Figure 5). However, after only a few cycles (2–3) the system becomes stable, the maximum voltages remain constant, and the pressure measurements are reproducible. With our experimental setup, we have observed a linear relationship between the applied pressure and the measured voltage for pressures up to 500 kPa. This data suggests that deformation of the graphene network in the composite is highly reversible, as it has also been observed for the starting graphene scaffolds.[11,16]

It is possible to use the material to prepare freestanding and flexible composite films with thicknesses below 500 μm (Figure 5d). These films can fully recover their shape from bending after the removal of external stress, and their electrical resistance depends on the degree of flexion, showing promise for flexion sensing applications. The resistance increases under flexion, however it goes back to lower values once the film is brought to the initial configuration. The cycle is fully repeatable (Figure 5e).

For natural and synthetic materials alike, one of the key issues is the critical volume of the flaw above which complete repair is not possible. In this respect, our results illustrate the advantages of confining a polymer able to flow at low stresses. However, to assure complete healing and large critical volumes we should maximize the healant content while retaining structural stability. The graphene network allows us to form a solid composite containing up to 99.8 wt% of a supramolecular polymer that behaves as a liquid at low strain rates. After damage, the polymer is released and due to its "solid–liquid" behavior flows to heal deep scratches or rejoin fracture surfaces and reform the conductive network at room temperature. Due to its dynamically bonded nature, the healing polymer is never exhausted and can act multiple times providing repeatable, autonomous recovery of mechanical and electrical properties.

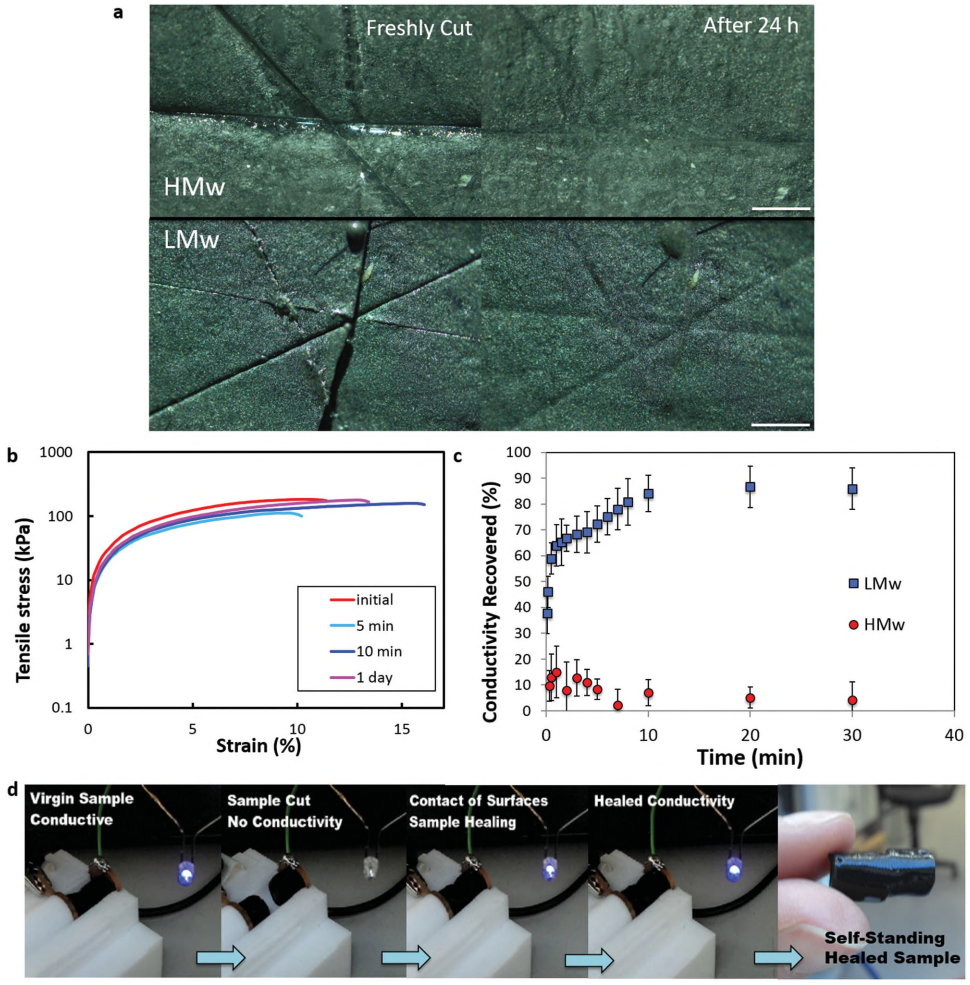


**Figure 4.** a) Optical microscopy images of deeply scratched composites obtained with HMw and LMw polymer and their physical healing after 24 h. b) Tensile stress–strain curves for original and healed samples after healing times ranging from 5 min to 1 d. Tensile tests carried out at 50 mm $min^{-1}$ strain rate. c) Recovery of electrical conductivity as a function of time for a sample with a starting conductivity of 55 S $m^{-1}$ with LMw polymer and a sample with a starting conductivity of 64 S $m^{-1}$ with HMw polymer both contain 0.5 wt% graphene. Almost complete electrical healing is obtained with LMw d) Demonstration of electrical healing by placing the composite (LMw PBS) in series with an LED. From left to right: original composites showing the passage of current though the conductive sample (LED is on); the drop in current (open circuit) when the sample is cut in half (LED is off) and the gradual recovery after the two surfaces are put back into contact with no pressure (LED is on and recovers the original light intensity after 10 min). Scale bars: (a) 1 mm.

The mechanical properties of the material allow the fabrication of bulk parts and films whose electrical conductivities can reach values up to 90 S $m^{-1}$ and that are sensitive to pressure and flexion. Being able to heal and sense external forces and deformation as a "synthetic skin," these materials could be of interest in the biomedical, robotic, and energy fields.

## Experimental Section

*Materials Synthesis*: Graphene oxide was prepared following the method described in[17] and its main properties are summarized in.[18] Graphene oxide suspensions in water with concentrations ranging from 15 to 30 mg $cm^{-3}$ were prepared using sucrose and polyvinyl alcohol (PVA) as additives (the GO:additive ratio was 1:2 in weight). The slurry was subsequently freeze-casted at a rate of 10 K $min^{-1}$ and freeze dried in a Labconco FreeZone 4.5 L console. The scaffolds obtained were reduced at 950 °C for 20 min in 10% $H_2$/90% Ar atmosphere inside a tubular oven. PDMS (25 cSt and 65 cSt Aldrich) and boron oxide nanoparticles ($B_2O_3$ SkySpring Nanomaterials, Inc., average size 80 nm) were vigorously mixed together in concentrations varying from 1 to 5 wt%, depending on the molecular weight of the polymer used, and infiltrated via vacuum casting inside the porous rGO networks with cylindrical (Vol ≈ 3.14 $cm^3$) or parallelepiped (Vol ≈ 16 $cm^3$) shape. The cross-linking reaction was carried out in the oven at 200 °C for 6 h. For rheological tests, a DHR3 rheometer from TA Instruments was used in both frequency swipe mode and amplitude swipe mode. For the samples with dispersed graphene flakes, reduced (as for the scaffolds) graphene oxide powder (obtained as described previously) was dispersed in PDMS, in concentrations up to 10 wt%, via ultrasonication tip (UP200S SciMed., UK) for 1 h with set amplitude of 50% and cycle 0.5. The solution was then cross-linked as described above.

*Materials Characterization*: The composite samples were tested in tension and compression under displacement control (Zwick Roell). Tensile tests were performed using dog-bone samples, with internal cross-sectional area of ≈0.12 $cm^2$. The conductivity of the sample was monitored in two-point via benchtop multimeter and in four-point probe configuration by using a power supply unit (PSU) with constant

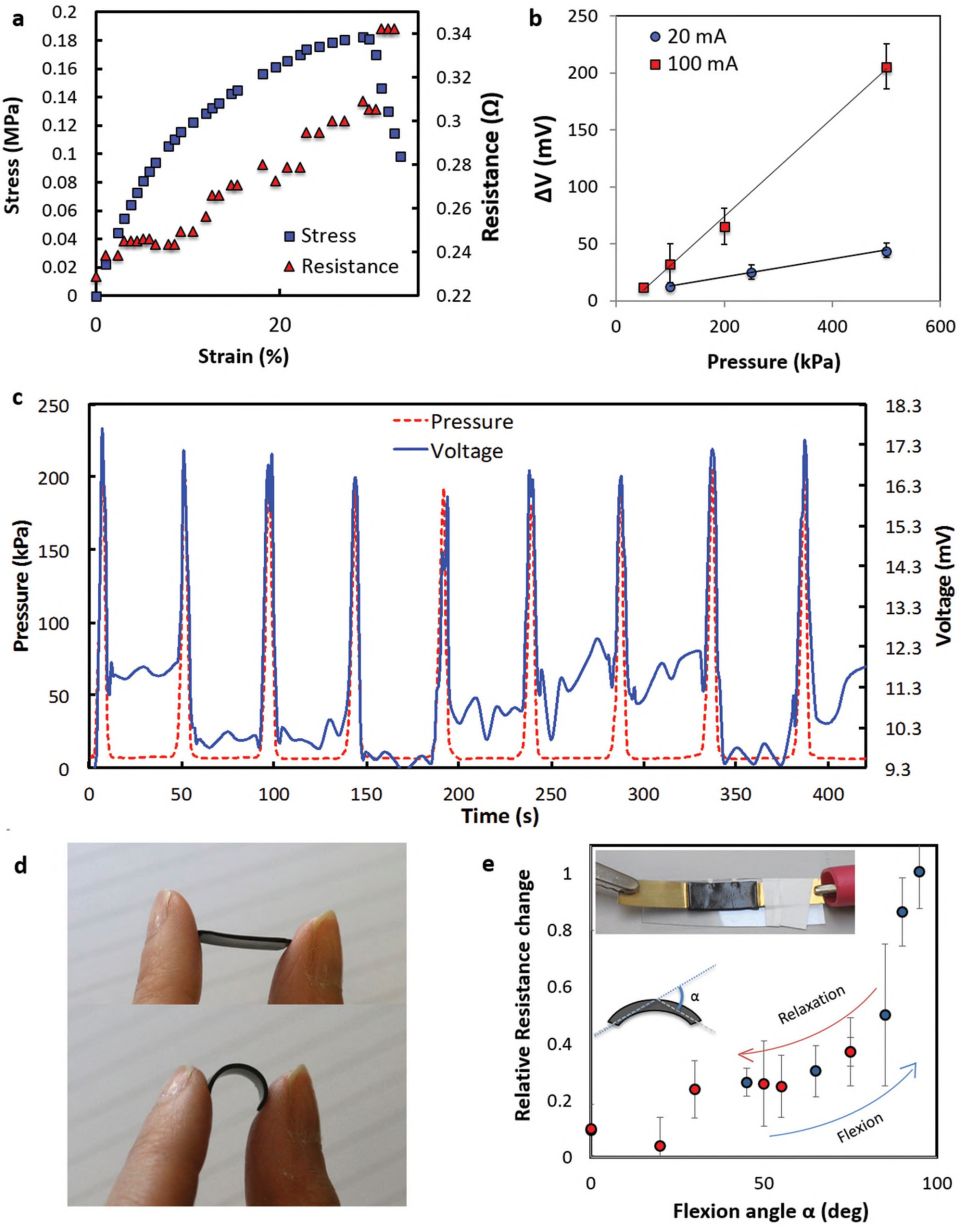


**Figure 5.** Sensing properties. a) Tensile-electric test recording the variation of resistance (in two-point probe configuration) with strain. The sample is still conductive after strains of 30%. Fracture and loss of electrical conductivity happen simultaneously. b) Dependence of the voltage increment with pressure for a measurement performed using the set up described in (c) with two different currents (20 and 100 mA). c) Pressure sensitivity. The voltage variation (in four-point probe configuration) is monitored under cyclic compression tests as a function of time. The composite has an LMw matrix with a graphene content of 0.5 wt%. Constant current: 20 mA, electrode distance 1.3 mm, sample length across 7.9 mm, and sample cross-sectional area 60 $mm^2$. d) Flexible films formed by the slicing of bulk composites into tapes less than 500 μm thick. The films are self-standing. e) Variation of resistance in two-point probe configuration of a 500 μm thick film flexed above 90°. The graph shows the effect of flexion and relaxation and the results have been repeated for three cycles without noticeable variations. The film recovers its initial resistivity after relaxation.

input current of 0.08 A and a standard four channels bench multimeter to measure the voltage variation. For the electrical tests, cylindrical samples were used as prepared and contacted to the circuit via copper electrodes. Films were cut out of parallelepiped (≈0.5 mm × 30 mm × 2 mm) structures and used in flexion conductivity tests by connecting the two opposite ends to the multimeter through flexible copper foil cut to shape. The films were bent manually while constantly monitoring the conductivity change with bending degree through a 30 fps camera. The microstructure of the porous networks was investigated by scanning electron microscopy (SEM) and aberration corrected transmission electron microscopy (FEI Titan 80-300 S/TEM, operated at 80 kV). Samples for SEM imaging were prepared by coating the surface with a 5 nm chromium layer and imaged using a 15 keV acceleration voltage (Zeiss CrossBeam workstation Auriga).

Due to the anisotropic structure of the starting graphene network, there is some expected dependence of the mechanical and electrical performance on the testing direction. The strength and conductivity measurements were taken in the direction parallel to the channels in the

graphene structure (the direction of ice growth during freeze casting). The measurement direction may affect some of the absolute values. For example, the storage modulus is higher in the direction parallel to the channels, whereas the electrical conductivity can be almost double in the perpendicular direction. However, the strength is similar in both directions as it is mostly dictated by the organic phase that comprises more than 98 wt% of the composites (Figures S2 and S3, Supporting Information).

## Supporting Information

Supporting Information is available from the Wiley Online Library or from the author.

## Acknowledgements

The authors would like to acknowledge the EPSRC grant Graphene 3D Networks (Grant No. EP/K01658X/1). S.B. and V.G.R. would like to acknowledge the European Commission (FP7 Marie Curie Intra-European Fellowships ACIN and GRAPES). E.D. would like to acknowledge EPSRC-DTA funding. N.N. would like to acknowledge EPSRC grant Engineering with Graphene for Multifunctional Coatings and Fiber-Composites EP/K016792/1.

[1] K. S. Toohey, N. R. Sottos, J. A. Lewis, J. S. Moore, S. R. White, *Nat. Mater.* **2007**, *6*, 581.
[2] a) B. C. K. Tee, C. Wang, R. Allen, Z. N. Bao, *Nat. Nanotechnol.* **2012**, *7*, 825; b) C. Y. Hou, T. Huang, H. Z. Wang, H. Yu, Q. H. Zhang, Y. G. Li, *Sci. Rep.* **2013**, *3,* 3138.
[3] a) N. Holten-Andersen, M. J. Harrington, H. Birkedal, B. P. Lee, P. B. Messersmith, K. Y. C. Lee, J. H. Waite, *Proc. Natl. Acad. Sci. USA* **2011**, *108*, 2651; b) P. Cordier, F. Tournilhac, C. Soulie-Ziakovic, L. Leibler, *Nature* **2008**, *451*, 977; c) X. X. Chen, M. A. Dam, K. Ono, A. Mal, H. B. Shen, S. R. Nutt, K. Sheran, F. Wudl, *Science* **2002**, *295*, 1698; d) M. Burnworth, L. M. Tang, J. R. Kumpfer, A. J. Duncan, F. L. Beyer, G. L. Fiore, S. J. Rowan, C. Weder, *Nature* **2011**, *472*, 334.
[4] M. W. Keller, S. R. White, N. R. Sottos, *Adv. Funct. Mater.* **2007**, *17*, 2399.
[5] M. M. Caruso, B. J. Blaiszik, S. R. White, N. R. Sottos, J. S. Moore, *Adv. Funct. Mater.* **2008**, *18*, 1898.
[6] a) G. M. L. van Gemert, J. W. Peeters, S. H. M. Sontjens, H. M. Janssen, A. W. Bosman, *Macromol. Chem. Phys.* **2012**, *213*, 234; b) R. Martin, A. Rekondo, A. R. de Luzuriaga, G. Cabanero, H. J. Grande, I. Odriozola, *J. Mater. Chem. A* **2014**, *2*, 5710; c) A. Zhang, L. Yang, Y. Lin, L. Yan, H. Lu, L. Wang*J. Appl. Pol. Sci.* **2013**, *129*, 2435.
[7] M. P. Goertz, X. Y. Zhu, J. E. Houston, *J. Polym. Sci. Polym. Phys.* **2009**, *47*, 1285.
[8] J. Li, J. K. Kim, *Compos. Sci. Technol.* **2007**, *67*, 2114.
[9] Z. Liu, *Ph. D. Thesis*, Delft University of Technology (The Netherlands) **2015**.
[10] S. Deville, E. Saiz, R. K. Nalla, A. P. Tomsia, *Science* **2006**, *311*, 515.
[11] N. Ni, S. Barg, E. Garcia-Tuñon, F. M. Perez, M. M. C. Lu, C. Mattevi, E. Saiz, *Sci. Rep.* **2015**, submitted.
[12] X. F. Li, D. A. Zhang, K. W. Xiang, G. S. Huang, *RSC Adv.* **2014**, *4*, 32894.
[13] A. Juhász, P. Tasnádi, L. Fábry, *Phys. Ed.* **1984**, *19*, 302.
[14] Z. Liu, S. J. Picken, N. A. M. Besseling, *Macromolecules* **2014**, *47*, 4531.
[15] D. Y. Wu, S. Meure, D. Solomon, *Prog. Polym. Sci.* **2008**, *33*, 479.
[16] S. Barg, F. M. Perez, N. Ni, P. D. V. Pereira, R. C. Maher, E. Garcia-Tuñon, S. Eslava, S. Agnoli, C. Mattevi, E. Saiz, *Nat. Commun.* **2014**, *5,* 4328
[17] D. C. Marcano, D. V. Kosynkin, J. M. Berlin, A. Sinitskii, Z. Z. Sun, A. Slesarev, L. B. Alemany, W. Lu, J. M. Tour, *ACS Nano* **2010**, *4*, 4806.
[18] E. Garcia-Tuñon, S. Barg, J. Franco, R. Bell, S. Eslava, E. D'Elia, R. C. Maher, F. Guitian, E. Saiz, *Adv. Mater.* **2015**, *27*, 1688.